Dynamics and Shear Orientation Behavior of a Main-Chain Thermotropic Liquid Crystalline Polymer

Wei-Jun Zhou and Julia A. Kornfield*

Chemical Engineering, 210-41, California Institute of Technology, Pasadena, California 91125

Victor M. Ugaz and Wesley R. Burghardt

Department of Chemical Engineering, Northwestern University, Evanston, Illinois 60208

Darren R. Link and Noel A. Clark

Department of Physics, University of Colorado, Boulder, Colorado 80309

Received March 17, 1999; Revised Manuscript Received June 2, 1999

ABSTRACT: The dynamics and shear orientation behavior of a model thermotropic liquid crystalline polymer (DHMS-7,9) were characterized by mechanical rheometry and *in situ* wide angle X-ray diffraction (WAXD). In the nematic phase (between 120 and 192 °C), DHMS-7,9 shows a three-region flow curve accompanied by a strong and relatively constant orientation over the entire shear rate range. A mysterious mesophase occurs between 92 and 120 °C that has much higher viscosity than that of the nematic phase and a monotonically shear thinning flow curve. In this phase, a striking flip of the orientation from the flow direction to the vorticity direction occurs below a critical shear rate. This orientational flipping is reversible in response to step changes of temperature and/or shear rate. Examination of the linear viscoelastic behavior suggests certain rheological similarities between the x-phase and layered fluids.

1. Introduction

Liquid crystalline polymers (LCPs) provide routes to high-performance materials with outstanding strengths and high use temperatures.[1] Thermotropic LCPs offer attractive processing characteristics relative to commercial lyotropes, which are processed from highly acidic solvents and are limited to fabrication of fibers. Thermotropes are amenable to a wider range of processes, including injection molding. In spite of the technological interest in thermotropic LCPs, most research has been directed to lyotropes.[2] Fruitful experimental approaches have been developed that combine model systems, rheology, and microstructural measurements.[3−5] Statistical mechanical models of rigid rods (the Doi theory) capture the essential features of the observed behavior of lyotropic LCPs.[6,7] Similar experimental and theoretical advances are needed for thermotropic LCPs.

Simple extension of the knowledge obtained from lyotropes to thermotropes is unlikely to hold. Thermotropes are not as rigid as most lyotropes. Further, intimate molecular contact in the melt state causes other intermolecular forces beyond a simple hard-rod potential to be important in governing their behavior. For example, while lyotropic LCPs generally show *director tumbling* under shear,[8,9] the limited results available on thermotropes suggest that at least some of them are *flow-aligning*.[10,11] Theoretically, an extension of the Doi theory that is more appropriate for semiflexible thermotropes (nematic dumbbell model) offers an explanation for flow-aligning behavior.[12] Yet such important characteristics as flow-aligning versus tumbling character have only been qualitatively established for a few thermotropes. Therefore, we pursue a coordinated experimental approach that combines scaled-up synthesis of a model thermotrope, rheological measurements, and synchrotron rheo-X-ray diffraction to clarify the relationship between structure and rheology. Here we focus on behavior in steady shear; subsequent papers address transient flow behavior, the effects of molecular weight, and rheo-conoscopic determination of the tumbling parameter.

As a point of departure for examining the shear behavior of thermotropes, it is useful to recall some key features of lyotropic LCP rheology. Among the unusual rheological phenomena observed in lyotropic systems are the so-called three-region flow curve,[13] negative values of the steady-state first normal stress difference (N_1),[14−17] and multiple oscillations in the transient stress response upon flow start up or a stepwise change of shear rate.[18,19] A three-region flow curve is comprised of shear thinning at low and high shear rates (regions I and III) and pseudo-Newtonian behavior (region II) at intermediate rates. The shear rate range in which negative N_1 is observed lies in the transition from region II to region III. Negative values of steady-state N_1 and multiple stress oscillations are attributed to director tumbling of lyotropic LCPs. The tumbling and associated rheological behavior have been successfully predicted by the Doi theory.[7]

Experimentally and theoretically, such a level of understanding is lacking for thermotropic LCPs. In relation to the variation of viscosity with shear rate, observed behavior includes completely shear thinning, shear thickening, and three-region flow curves.[20,21] Regarding the occurrence of sign changes in the first normal stress difference, it has been suggested that all reported negative values of the steady-state N_1 in thermotropes are due to experimental artifacts.[22] The multiple oscillations of transient shear stress, common

* To whom correspondence should be addressed. E-mail: jak@cheme.caltech.edu.

10.1021/ma990399f CCC: $18.00
Published on Web 07/30/1999

in lyotropic LCPs upon sudden change of shear rate, have not been observed in thermotropes. The absence of multiple oscillations suggests flow-aligning character. Initial attempts to include the effects of flexibility predict that semiflexible nematic chains tend to be flow aligning.[12,23−25] To fully understand the rheology of thermotropes, further information on the flow curve (both for the viscosity and N_1) and the underlying molecular orientation during flow is needed.

The relative dearth of information on the structure and rheology of thermotropic LCPs reflects multiple levels of experimental difficulties associated with these materials. Commercial thermotropes usually have an inaccessible isotropic−nematic transition temperature and often undergo transesterification at temperatures in the nematic range (at $T > T_m$ with typical $T_m \approx 300$ °C). Thus, the sample continuously changes over the course of measurements.[20,26] The inability to erase prior thermal and flow history strongly affects the measurement and interpretation of bulk rheological data. In addition, most thermotropes are too turbid for optical techniques to be used in characterizing molecular orientation or microstructure during flow, which accounts for the relatively small number of rheo-optical studies on thermotropic LCPs.[27,28] This has motivated development of model materials with accessible isotropic transitions ($T_{ni} < 210$ °C) and good optical transparency, including a number of polyesters and a polyether.[29−31] We choose the latter type because of its greater thermal stability (no transesterification).

The thermotropic polyether based on a dihydroxymethylstilbene (DHMS) mesogen developed by Percec has been proven to be a good model system for rheological characterization.[31,32] In this study, we examine DHMS-7,9, in which DHMS is copolymerized randomly with seven and nine methylene spacer groups (Chart 1). As a model system, DHMS-7,9 offers an accessible isotropic state, a stable chemical structure, a modest melting point with a wide nematic range, and good optical transparency. DHMS-7,9 exhibits a nematic phase between 120 and 192 °C and an unusual mesophase ("x-phase"[32]) between 92 and 120 °C. The linear viscoelastic behavior of DHMS-7,9 has been studied by Gillmor and co-workers, who found the viscoelastic properties of the nematic phase are controlled by the large-scale defect structure.[32]

Our primary objective is to establish the relationship between bulk rheological properties (viscosity and N_1 versus shear rate) and microstructure (the degree and direction of molecular orientation) in steady shear. The results of this approach reveal that, in the nematic phase, DHMS-7,9 shows a three-region flow curve accompanied by a strong and relatively constant orientation along the flow direction over the entire shear rate range. This relationship between viscosity and orientation is quite unlike that for lyotropes, suggesting that the explanation of the three-region flow curve may be different for this thermotrope. The x-phase brings more complex orientational behavior, particularly a flip of orientation from the vorticity direction at low shear rates to the flow direction at high shear rates. This orientational flipping is reversible in response to step changes of temperature across T_{xn} and of shear rate across the critical value $\dot{\gamma}_c(T)$. The ability to create differently aligned states allows us to examine their linear viscoelastic characteristics; these provide different signatures for the nematic and x-phases. The implications of these observations for current concepts regarding the rheology of LCPs and the mystery of the x-phase are examined in the Discussion.

Chart 1. Chemical Structure of DHMS-7,9

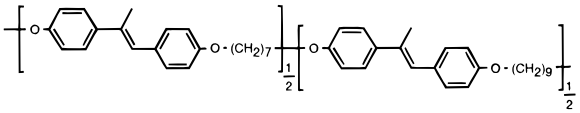

2. Experimental Section

2.1. Materials. The thermotropic polymer used here is a random copolyether of mesogen DHMS coupled with two different lengths of alkyl spacers (7- and 9-methylene) to suppress its melting point (Chart 1). The synthesis protocol was modified from the methods described in the literature.[31] DHMS-7,9 was precipitated from methanol and heptane alternately, while only methanol was used by Percec. Batches of 100 g have been synthesized to provide sufficient quantities of material for systematic rheological, X-ray, and microscopy studies. The molecular weights of the polymer were determined by GPC using polystyrene standards in CH_2Cl_2 solution. This study will focus on the sample with a polystyrene-equivalent $M_w = 28\,440$ g/mol and a polydispersity around 2.3.

Differential scanning calorimetry (Perkin-Elmer DSC7) was used to determine phase transitions using a rate of 10 °C/min during both heating and cooling under an argon purge. Polarized light microscopy (Zeiss Universal Pol-Microscope equipped with Mettler FP-80 hot stage) was used to characterize liquid crystalline texture and mesophase transitions.

2.2. Powder X-ray Diffractometry. Powder X-ray diffraction was carried out on NSLS beamline X10A. A germanium monochromator was chosen for its high resolution of 0.0007 $Å^{-1}$. Samples were contained in 1 mm diameter thin wall quartz capillaries inside an aluminum oven with temperature control. Data are presented as X-ray counts (intensity) normalized by the incident monitor count rate.

To examine the mesophase behavior of DHMS-7,9, the sample was first heated to the isotropic state (205 °C) for 20 min and then slowly cooled into the nematic phase (or x-phase) and allowed to equilibrate for at least 30 min before measurements. We also investigated thermal hysteresis of the phase behavior by heating the sample from room temperature directly to each desired temperature in the x-phase (or nematic phase) without going to the isotropic state. Diffraction measurements were obtained on these samples after 30 min of thermal equilibration.

2.3. Rheological Measurements. The polymer as synthesized above is in either fibrillar or powder form. Specimens for rheological measurements were prepared by solvent casting. DHMS-7,9 was dissolved in $CHCl_3$ in the presence of 0.75% antioxidant (octadecyl 3-(3,5-di-*tert*-butyl-4-hydroxyphenyl)propionate, 99%, Aldrich Chem., Inc.). The solvent was evaporated slowly from the polymer solution at room temperature for a few days. The cast polymer film was then dried for at least 24 h under vacuum (<1 mmHg) at 80 °C. Samples were subsequently fabricated into 25 or 50 mm disks with 1 mm thickness by molding in a heated press at 140 °C. Before the sample was loaded into a rheometer, the molded disk was further dried under vacuum overnight at 80 °C to remove moisture. This sample preparation avoids possible voids in the sample. These procedures have proven to give reproducible rheological data. We did not see evidence of significant offgasing problems as reported by Kalika and co-workers,[21] which is a typical concern for thermotropic polyesters. DHMS-7,9 was thermally stable in the nematic phase for at least 3−4 days without a discernible change of the linear viscoelastic response. This enables prolonged rheological measurements. We are thus able to examine steady shear flow behavior even at rather low shear rates ($\dot{\gamma} \leq 0.01$ s^{-1}).

The Rheometrics ARES rheometer (equipped with a 2000 g·cm transducer) was used for most rheological measurements. The polymer sample is heated using a forced convection

heating oven (up to 400 °C) with temperature stability to ±0.2 °C. All of our experiments were performed under continuous dry nitrogen purge to prevent oxidative and hydrolytic degradation. We heated the sample to 205 °C (isotropic state) and held it for 20 min to erase the prior mechanical and thermal history. The sample was then cooled to the desired temperature in the nematic phase (or x-phase) with an additional 30 min of thermal equilibration time before commencing flow experiments. *In situ* flow X-ray studies followed the same experimental protocol.

A parallel-plate geometry (diameter = 50 mm, gap = 1 mm) was used in studying the temperature dependence of the apparent shear viscosity at a fixed rim shear rate. Measurements were performed at temperatures spaced every 5 °C over the interval of 100−200 °C. For each measurement, the samples were presheared for 150 s.u. (strain units) at the sample rim to attain steady state before data collection. The same sample geometry was employed for dynamic temperature sweep experiments because it is easier to compensate for thermal expansion of the tool fixtures (≈3 μm/°C) in the parallel-plate configuration than in the cone-and-plate geometry.

Oscillatory dynamic data were collected as a function of angular frequency (ω). A parallel-plate geometry (diameter = 50 mm, gap = 1 mm) was used for randomly oriented samples. The strain amplitude (at the rim) varied from 1% to 30% at frequencies between 100 and 0.01 rad/s. It was verified that linear viscoelastic response holds over this range of strain amplitude. Little difference was observed when a cone-and-plate configuration was used. For dynamic measurements in well-oriented states (obtained by preshearing at selected shear rates), cone-and-plate fixtures (diameter = 25 mm, cone angle = 0.1 rad) were used in order to achieve uniform shear throughout the whole sample during preshear.

Measurements of the steady shear viscosity (η) and the first normal stress difference (N_1) were also conducted in the cone-and-plate configuration: 25 mm diameter and 0.1 rad cone angle for the x-phase and 50 mm diameter and 0.04 rad cone angle for the nematic phase. The ARES rheometer was used to investigate shear rates in the range 0.01−10 s^{-1}. Measurements at lower shear rates ($\dot{\gamma}$ < 0.01 s^{-1}) were performed on the Rheometrics stress rheometer (SR-5000) equipped with a more sensitive transducer (100 g·cm). Melt fracture was observed at shear rates above 10 s^{-1} in the nematic phase.

A sample-loading procedure was developed specifically for rheological measurements in the x-phase. The molded sample disk was first placed on the 25 mm plate and then heated to 140 °C. We reduced the center gap thickness to about 250 μm at 140 °C after thermal equilibration. Then we heated the sample to the isotropic state while simultaneously adjusting the gap to keep the normal force small (≤10 g). After the sample was thermally cleared, we cooled it slowly to the x-phase while constantly adjusting the gap thickness. After about 5 min of thermal equilibration in the x-phase, we adjusted the final center gap gradually to about 50 μm. It usually takes several hours to relax the normal force caused by the squeezing flow during the final gap setting in the cone-and-plate configuration.

2.4. Rheo-X-ray Protocol and Data Analysis. The rheo-X-ray flow cell is a modified Linkam CSS-450 high-temperature shearing stage; the details have been described elsewhere.[11] The unit provides a parallel disk shearing geometry. A sample thickness of 1 mm was used. All X-ray experiments were conducted on beamline 5-BM at the Advanced Photon Source (APS) of Argonne National Lab. The beam diameter is 0.4 mm, and the energy of incident radiation was 25 keV (λ = 0.621 Å). The resulting scattering pattern is collected on a two-dimensional wire detector, which reflects the projection of the flow-induced molecular orientation in the flow−vorticity plane (1,3-plane).

This scattering pattern was digitized and analyzed to characterize the degree and direction of molecular orientation. Following the analysis of Mitchell and Windle,[33] a 2-D orientation parameter (S) can be calculated by taking the average of the second Legendre polynomial $\langle P_2 \rangle$, weighted by an azimuthal intensity scan $I(q,\phi)$, where q denotes the scattering vector. The azimuthal angle ϕ is measured from the flow direction or the vorticity direction, depending on the direction in which molecules are preferentially oriented. S is computed by normalizing $\langle P_2 \rangle$ obtained from the 2-D scattering pattern to the ideal case of perfectly aligned rods. Thus, its value ranges from zero (no preferred orientation) to one ("perfect" orientation along a given direction).

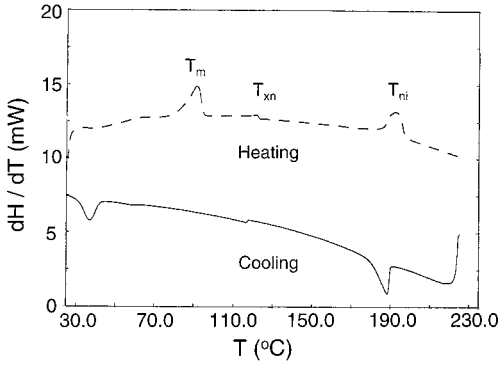

Figure 1. Differential scanning calorimetry traces for DHMS-7,9 (M_w = 28 kg/mol). The temperature scanning rate was 10 °C/min for both heating and cooling, and the amount of sample used was 10 mg.

3. Results

3.1. Phase Behavior. DHMS-7,9 (M_w = 28 440 g/mol) undergoes phase transitions at 92, 120, and 192 °C (Figure 1). The transition at 92 °C on heating has been assigned to the melting of the polymer; this transition shows large thermal hysteresis, with crystallization occurring at approximately 35 °C on cooling (10 °C/min). The upper transition coincides with the isotropization point (192 °C) observed by polarized light microscopy. Between 120 and 192 °C, a typical Schlieren texture was observed, which indicates that DHMS-7,9 is nematic in this temperature region. It also displays an intermediate mesophase between the crystalline solid and nematic phase. However, no clear texture can be identified in this temperature range under a polarized light microscope. Because of its mysterious nature, this regime is referred as the "x-phase", following the same notation as that used in previous literature.[34] The nematic−isotropic biphasic region is rather broad. This is attributed to the wide distribution of molecular weight for DHMS-7,9. On the other hand, the x−nematic transition occurs within a much sharper temperature range, suggesting this transition is less sensitive to the molecular weight distribution of polymers. In addition, the x−nematic transition appears at nearly the same temperature during heating and cooling. Previous studies of DHMS-7,9 have shown that the transition temperatures vary with chain length and polydispersity; the observed transitions for the present 28 kg/mol sample fall within the previously reported range.[34]

To examine the nature of the intermediate x-phase, high-resolution powder X-ray diffraction has been performed. Upon cooling from the isotropic state, the isotropic−nematic transition is manifested by the growth of a broad diffraction peak in $I(q)$ at $q \approx 1.25$ $Å^{-1}$ (Figure 2a, 166, 150, 135 °C). This liquid-like diffuse peak is characteristic of interchain packing correlations. The peak position shifts out with decreasing temperature, varying from $q \approx 1.2$ to 1.4 $Å^{-1}$, corresponding to effective interchain spacings ranging from 5.5 to 4.5 Å. On moving from 135 to 119 °C to 106 °C and 96 °C, the

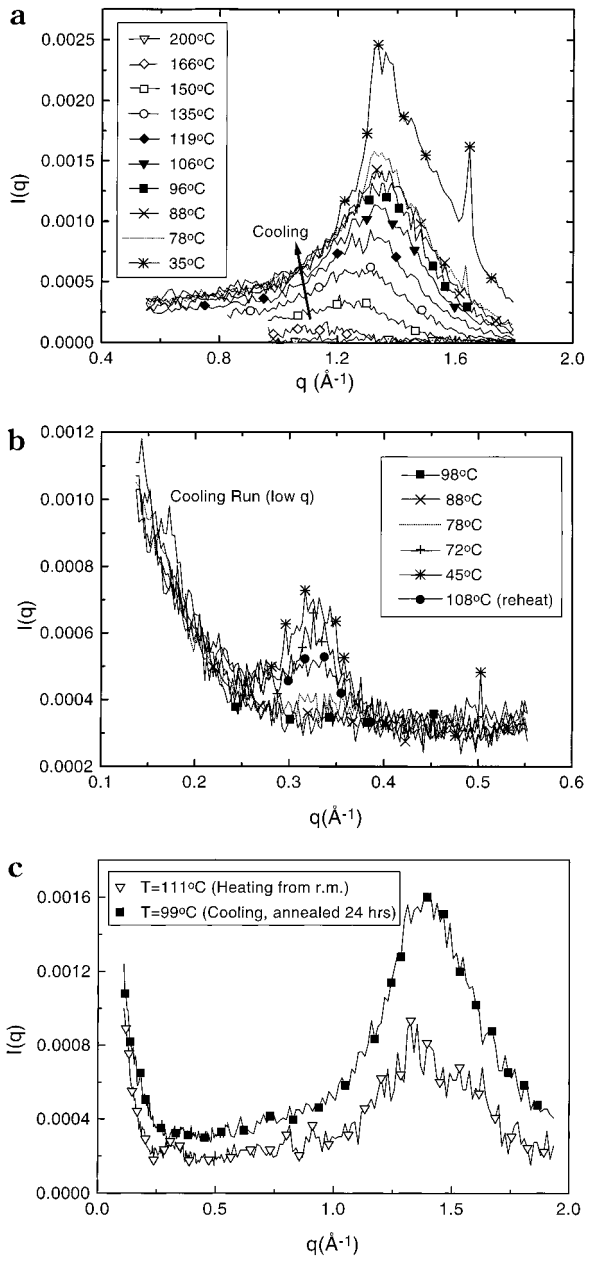

Figure 2. X-ray diffraction intensity $I(q)$ versus q of DHMS-7,9 (M_w = 28 kg/mol) at different temperatures: (a) cooling runs at large q; (b) cooling runs at small q, including a reheat run from room temperature at 108 °C; (c) a heating run from room temperature at 111 °C and a cooling run at 99 °C with annealing for 24 h.

interchain correlation peak simply shows the usual increase of intensity and slight shift to larger q that are typical for the nematic phase with decreasing temperature. Thus, there is no evidence of a more ordered structure (compared to nematic order) forming when cooling through the x-phase (120−92 °C). Higher order structure first appears at much lower temperature. A sharp diffraction peak at $q \approx 1.65$ Å^{-1} is evident at 78 °C and below (Figure 2a), attributed to crystallization at low temperatures. In addition, a small angle peak characteristic of crystal-like layer ordering appears at $q \approx 0.32$ Å^{-1} upon crystallization during cooling (at T = 78, 72, and 45 °C, Figure 2b). This peak corresponds to a layer spacing of 19.6 Å and has no observable harmonics,[35] as is common for either the layer ordering of smectic LCs or the lamellar superstructure of semicrystalline polymers. The finite peak width of about 30 times the diffractometer resolution suggests such layering is short ranged. The correlation length obtained from fitting the peak to a Lorentzian line shape is about 58 Å.

In principle, such layer ordering could be crystalline or smectic. Our observation rules out the possibility that the x-phase is *purely* smectic for at least two reasons. First, this layering peak is about a factor of 10 smaller in integrated intensity than that observed for a typical smectic LC in the same sample geometry, suggesting that only a small part of the sample adopts layer ordering. Second, the sample showed a rather large structural hysteresis in the x-phase: upon heating from room temperature, the small q scattering peak ($q \approx 0.32$ Å^{-1}) persists with increasing temperature (Figure 2c). Smectics do not show such hysteresis. It must be emphasized that by X-ray diffraction the x-phase is not distinguishable from the nematic phase when the sample is cooled from the isotropic state. Even when the sample was annealed at 99 °C for 24 h after cooling from the isotropic state, no small q scattering peak other than that associated with nematic ordering was observed, as shown in Figure 2c. Therefore, we will refer to the above-mentioned layer ordering as *residual order*, since it occurs only when the sample is heated from room temperature into the x-phase but *not* for the case when the sample is cooled from the isotropic state to the x-phase.

There is a smooth background scattering, monotonically increasing with decreasing q, in the scattering profile as $q < 0.25$ Å^{-1} (Figure 2). This is definitely due to the DHMS-7,9 sample, since the empty cell or a typical smectic LC produces only a flat background at the intensity 2×10^{-4}. The monotonic background is characteristic of random spatial variations in density. A curve fit of the background to a constant plus a power law component works well, giving a variation with q as $q^{-\nu}$, with $\nu \approx 2$. This fall off with q is indicative of density fluctuations having Ornstein−Zernike type spatial correlations. We suspect that the origin of this background is due to some kind of nonhomogeneous spatial organization of the polymer. In particular, it may arise from heterogeneity associated with the statistics of incorporation of seven and nine methylene spacers in the polymer chain.

Further insight into the phase transitions is gained by examining the rheological properties of DHMS-7,9. The temperature dependence of the apparent steady shear viscosity at a fixed rim shear rate (0.1 s^{-1}) shows pronounced changes associated with the x−nematic and nematic−isotropic transitions (Figure 3). With an increase of temperature from 100 °C, a dramatic drop in viscosity is apparent at $T \approx 120$ °C (Figure 3), which coincides with the x−nematic transition, as evident by DSC. The apparent shear viscosity in the nematic phase is more or less constant, decreasing slightly with an increase of temperature for 120 °C < T < 170 °C. An increase in the apparent viscosity at 170 °C < T < 185 °C suggests entrance of the nematic−isotropic biphase region. The apparent viscosity decreases again with temperature when the sample is fully isotropic. The nematic−isotropic biphase region is very wide with an onset temperature around 175 °C. For comparison, the complex viscosity as a function of temperature was also measured (at ω = 5 rad/s, rim strain amplitude = 5%). It showed the same broad nematic−isotropic

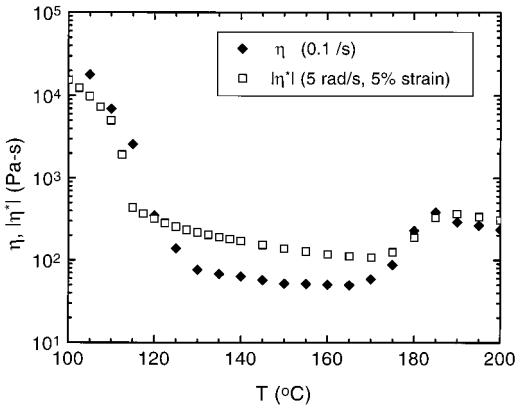

Figure 3. Apparent shear viscosity versus temperature: steady shear viscosity (η) was obtained at a rim shear rate of 0.1 s^{-1}, while complex viscosity ($|\eta^*|$) data were measured at a frequency of 5 rad/s with a 5% rim strain amplitude. Both measurements were conducted on 50 mm parallel plates with a 1 mm gap thickness.

transition. The x−nematic transition determined from the complex viscosity shifted slightly to a lower temperature and was very sharp. The phase transitions as indicated by rheology agree with the DSC data (Figure 1).

3.2. Rheological Behavior. We examined the linear viscoelastic and steady shear behavior of the isotropic, nematic, and x-phases. First, we describe the dynamic moduli of the unoriented state; comparison to the well-oriented mesophase is made in section 3.4. Then we present the viscosity and the first normal stress difference characteristic of each phase in steady shear. The transient rheology will be presented elsewhere.[36]

3.2.1. Oscillatory Shear Flow. In the isotropic phase, the linear viscoelastic response of DHMS-7,9 is different from that of simple flexible polymers. The dynamic moduli do not show characteristic terminal behavior at any of the temperatures studied (Figure 4a). Both the storage and loss moduli are roughly proportional to $\omega^{0.85}$ at low frequency in the isotropic phase. This agrees with Gillmor and co-workers' studies on the same system with slightly higher M_w[32] but differs from Kim and Han's studies on thermotropic polyester (PSHQ),[29] where no difference from flexible polymers was observed in the isotropic state. It is not clear why the terminal regime is absent for DHMS-7,9, but the possibility of a remnant birefringent structure in the isotropic state suggested by Gillmor and co-workers was excluded by direct observation through a polarized light microscope in the present case.

In the nematic phase, time−temperature superposition nearly holds for DHMS-7,9 with a random polydomain orientation. Departure from time−temperature superposition is most evident at the low frequency in the vicinity of T_{ni} (Figure 4a). Approximate shift factors are determined by shifting along the frequency axis alone until the storage and loss moduli at high frequency roughly superpose. The change in the shape of the relaxation spectrum with temperature is not monotonic (Figure 4a). On cooling, the storage modulus at low frequency first drops (starting at $T \approx T_{ni} + 20$ °C). This drop is most significant at the isotropization point ($T = 192$ °C). Then G' rises as the temperature drops to $T \approx T_{ni} - 10$ °C. Once the transition is complete ($T \leq 175$ °C), G' approximately superposes with G' of the isotropic phase at 220 °C. Like the case of the

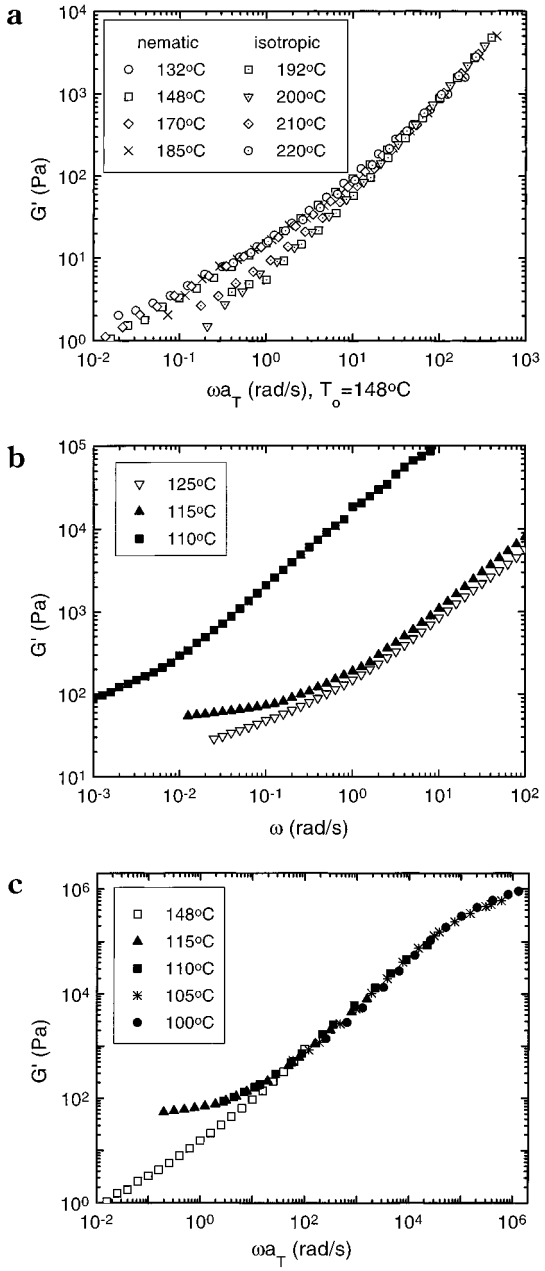

Figure 4. Storage modulus as a function of frequency. In parts (a) and (c), measurements at different temperatures have been shifted along the frequency axis alone to achieve approximate superposition at high frequency: (a) in the nematic and isotropic phases; (b) in the vicinity of the nematic−x phase transition; (c) in the x-phase (with nematic phase data at $T =$ 148 °C for comparison).

isotropic phase, no terminal response for G' was observed in the nematic phase. The absence of the terminal regime has also been reported for the same DHMS-7,9 system with different M_w[32] and other thermotropic systems.[29,30] This could be attributed to the effect of the large-scale defect structure, as suggested by Gillmor and co-workers.[32]

When the x-phase is reached, the storage modulus increases by about 2 orders of magnitude (Figure 4b). Alternatively, this enhancement in G' can be viewed as a dramatic slowing down of dynamics. Power law behavior is not exhibited in the x-phase; instead a plateau-like modulus occurred at low frequencies ($\omega \approx$ 0.1 rad/s at 115 °C). The storage modulus also follows an approximate $t-T$ superposition for all the temper-

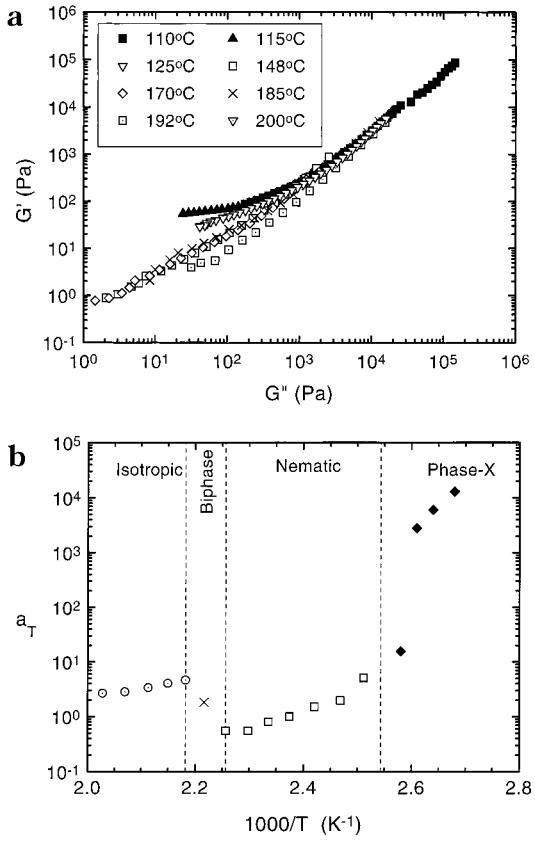

Figure 5. (a) Cole−Cole plots (log G' versus log G'') at different temperatures; (b) shift factors versus 1000/T in the isotropic, nematic, and x-phase (reference temperature: 148 °C).

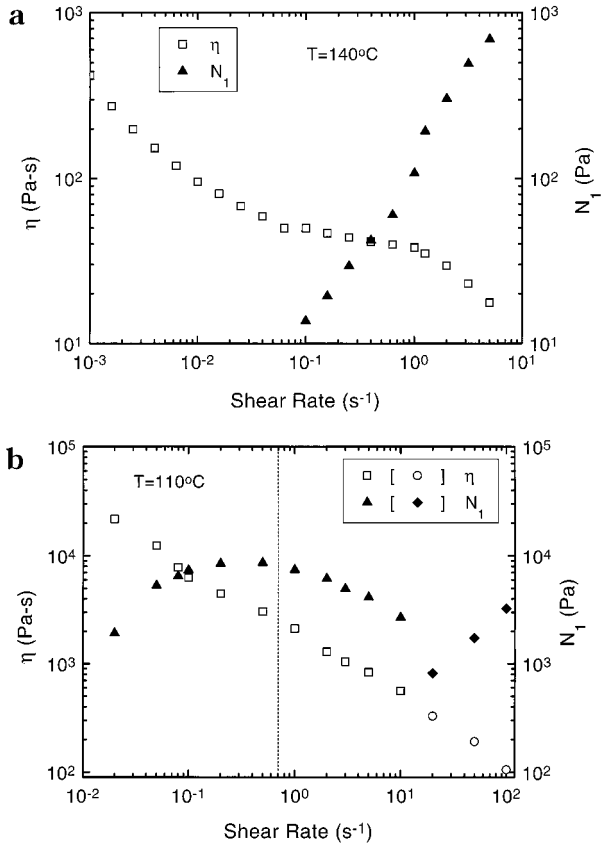

Figure 6. Steady shear viscosity (open symbols) and first normal stress difference (filled symbols) as a function of shear rate at two temperatures: (a) 140 °C (nematic phase) and (b) 110 °C (x-phase). Open circles and filled diamonds ($\dot{\gamma} > 10$ s^{-1} at 110 °C) indicate apparent η and N_1 under conditions of mild edge fracture. Vertical line indicates $\dot{\gamma}_c$ at 110 °C (see text and Figure 8).

atures in the x-phase (Figure 4c), with a small overlap in G' between the nematic (148 °C) and the x-phase.

A Cole−Cole plot (log G' versus log G'') can reveal departure from $t-T$ superposition without the uncertainty associated with arbitrary shifting factors. At high modulus values, plots of log $G' \sim$ log G'' in the isotropic, nematic, and x-phases fall almost on the same curve with small deviations, but at low modulus, the curves for different phases are distinct (Figure 5a). This is not unexpected, since linear viscoelasticity at high frequency is mainly governed by local chain dynamics. The Cole−Cole plots at different temperatures within the same phase nearly follow the same curve, which justifies the approximate time−temperature superposition used above. The log G' versus log G'' curves for the x-phase lie above those of the isotropic and nematic phases, with the occurrence of a small plateau at low G''. The Cole−Cole plots for the nematic phase also lie above those of the isotropic phase. This could be attributed to the distortional elasticity related to the defect structure in the nematic phase, which leads to an enhancement of the storage modulus and therefore a long relaxation tail at low oscillatory frequency. The curve for the nematic−isotropic biphase at 185 °C follows those of the isotropic state at high G'' values (in accord with the isotropic phase being the continuum matrix) but has slightly higher G' at low frequency (or low G'') values, which may be due to the distortion of the dispersed nematic droplets.

The shift factors exhibited Arrhenius dependence in the isotropic and nematic phases (Figure 5b). The approximate shift factors (a_T) that provide the best superposition at high modulus show abrupt changes in the vicinity of the isotropic−nematic and nematic−x−phase transitions. The large increase of a_T in the x-phase again indicates much slower dynamics. The flow activation energies of the isotropic and nematic phases are roughly equal, but much lower than that of the x-phase.

3.2.2. Steady Shear Flow. In the nematic phase, the shear stress (σ) reaches steady state at about 100 s.u. after flow inception. The stress curve usually exhibits a large overshoot and then decays away to steady state. Unlike the case for lyotropic systems,[8] no multiple oscillations were observed for flow start up. The viscosity curve (η versus $\dot{\gamma}$) is consistent with the typical three-region flow behavior (Figure 6a): shear thinning at low rates ($\dot{\gamma} < 0.05$ s^{-1}), pseudo-Newtonian at intermediate rates (0.05 s$^{-1} < \dot{\gamma} < 1$ s^{-1}), and shear thinning again at high rates ($\dot{\gamma} > 1$ s^{-1}). No qualitative change in the shape of the flow curve with temperature was observed within the nematic phase.

The first normal stress difference (N_1) required a longer shearing time (about 250 s.u.) to arrive at its steady-state value in the nematic phase. Temperature fluctuations lead to fluctuations in the normal force over the course of measurements. The data reported here are time averages over 100 s.u. after N_1 reaches steady state. At shear rates below 0.1 s^{-1}, the first normal stress difference is below the sensitivity of our instrument. N_1 is positive at shear rates above 0.1 s^{-1} and grows nearly proportionally with the applied shear rate. No reproducible N_1 data could be obtained at shear rates above 10 s^{-1} in the nematic phase due to edge fracture.

The steady shear viscosity and first normal stress difference behave very differently in the x-phase. It takes a longer time for the shear and normal stresses to reach steady state in the x-phase than in the nematic phase. Shear thinning dominates over the entire range of shear rates studied (Figure 6b), and no plateau region was observed. The viscosity is roughly two orders of magnitude higher in the x-phase than in the nematic phase, as expected on the basis of the linear viscoelastic properties.

In the x-phase, N_1 is positive for all the shear rates. There is an appreciable first normal stress difference even at shear rates as low as 0.02 s^{-1} (Figure 6b). The change of N_1 with shear rate is not monotonic. It first increases with shear rate and reaches a local maximum at $\dot{\gamma} \approx 2.5$ s^{-1}; then N_1 decreases with further increase of the shear rate and reaches a local minimum at $\dot{\gamma} \approx 20$ s^{-1}. N_1 increases again at higher shear rates ($\dot{\gamma} > 20$ s^{-1}). Slight edge fracture occurs at a shear rate around 20 s^{-1}. This can be suppressed by shearing samples at low shear rates (0.02 s^{-1}) before commencing high shear rate flow. According to the results of Baek et al. on highly concentrated hydroxypropylcellulose (HPC) solutions, mild edge fracture does not change the qualitative trend (increase or decrease) of N_1 measurements.[37]

3.3. Molecular Orientation during Steady Shear. *In situ* wide angle X-ray diffraction was performed with the incident X-ray beam parallel to the velocity gradient, as described in the Experimental Section. Thus, the 2-D scattering pattern contains information on the projection of the 3-D molecular orientation distribution on the flow−vorticity plane. During steady shear two qualitatively different types of pattern were observed. One is indicative of mesogens predominantly oriented along the flow direction ("parallel"), and the other is for mesogens with their preferential orientation along the vorticity direction ("perpendicular"). The magnitude of S was computed with different reference axes for parallel and perpendicular orientations, along the flow direction and the vorticity direction, respectively. In this way, computed S values are always positive, reflecting the degree of alignment relative to the prevailing orientation direction. In presenting results here, positive values of S are used to denote molecular orientation in the parallel orientation state, while negative values of S denote orientation in the perpendicular orientation state. The degree and direction of the molecular orientation depend on temperature and shear rate (T, $\dot{\gamma}$). Thermal history also appears to affect shear orientation behavior, as described below.

3.3.1. Effect of Temperature and Shear Rate. Comparison of the 2-D orientation parameter (S) and the corresponding shear viscosity (η) as a function of temperature shows the correlation between the change in the molecular orientation and the macroscopic flow properties (Figure 7). An orientation transition from perpendicular to parallel occurs as temperature increases through the x-nematic phase transition. This transition coincides with a dramatic decrease in viscosity with temperature. The degree of the molecular orientation is more or less constant throughout the whole nematic range. As the temperature approaches the nematic−isotropic transition, the orientation parameter decreases to zero over the same temperature range where the increase in shear viscosity is observed.

The shear-rate dependence of S is qualitatively different in the nematic and x-phases (Figure 8). At

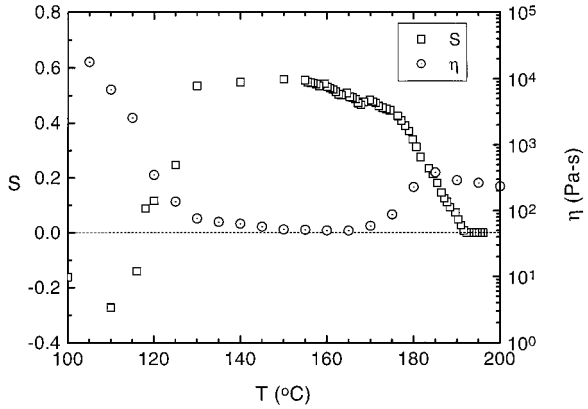

Figure 7. 2-D orientation parameter (S) and apparent shear viscosity, as a function of temperature at a single shear rate (0.1 s^{-1}). Negative values of S are used to represent data with the vorticity direction as the azimuthal coordinate. At least 150 s.u. preshear was applied to the sample to achieve steady state.

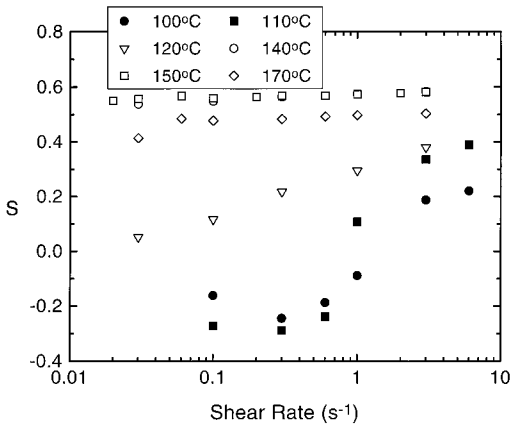

Figure 8. Orientation parameter (S) as a function of shear rate at temperatures in both the nematic phase and the x-phase. Negative values are used to represent data with the vorticity direction as the azimuthal coordinate.

temperatures well within the nematic phase (140, 150, 170 °C), there is little change in orientation with shear rate. This simple orientation behavior changed dramatically at temperatures near and below the transition to the x-phase. At 120 °C (T_{xn}), a monotonic increase of orientation with the applied shear rate was observed and the final orientation is relatively low compared to that for the nematic phase. Below T_{xn}, there exists a critical shear rate $\dot{\gamma}_c$, below which perpendicular orientation ($S < 0$, along the vorticity direction) was observed and above which the orientation flipped back to the flow direction ($S > 0$). A progressive change from the perpendicular to the parallel orientation is evident with the increase of the shear rate through $\dot{\gamma}_c$ in the x-phase (Figure 8).

3.3.2. Regimes of Parallel and Perpendicular Orientations. To establish the conditions that lead to the parallel and the perpendicular orientations, extensive *in situ* flow-X-ray experiments were conducted in both the nematic phase and the x-phase to map out the steady-state orientation as a function of temperature and shear rate. In the nematic phase, only the parallel orientation was observed (Figure 9). The degree of orientational order depends very weakly on the applied shear rate and the temperature except in the vicinity of T_{xn} and T_{ni}. In the x-phase, there are two orientation states

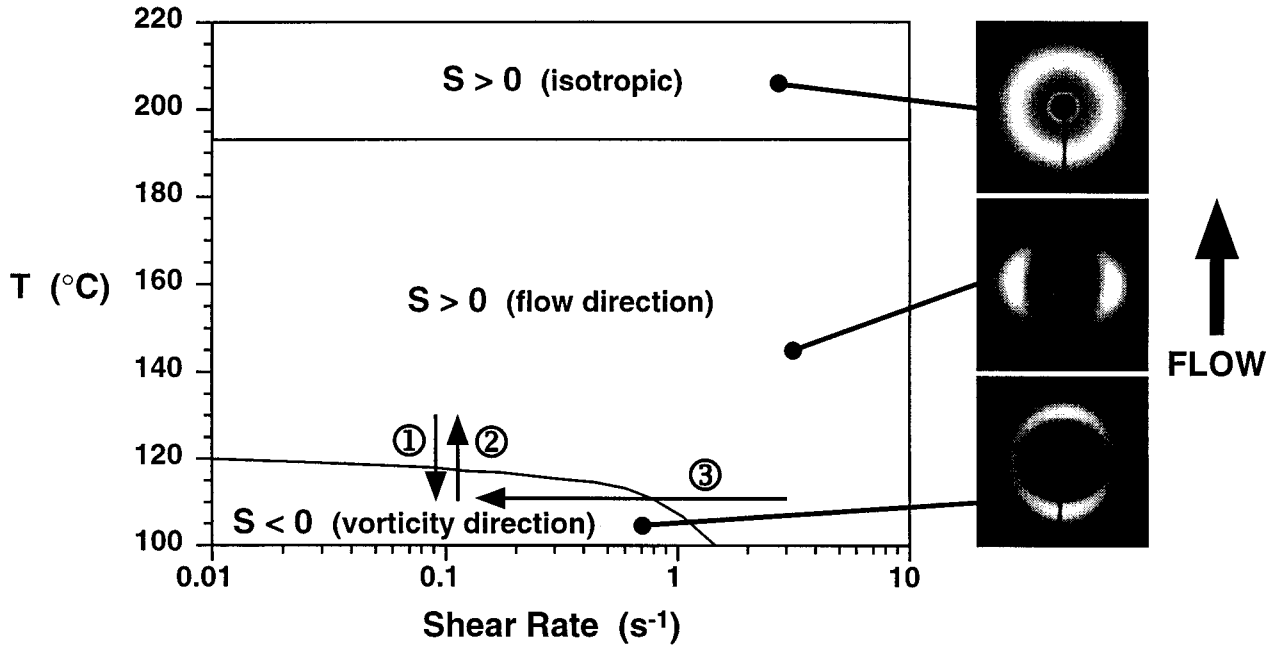

Figure 9. Mapping diagram of molecular orientation (S) in temperature−shear rate space. Three representative diffraction patterns for the isotropic phase (no net alignment), the parallel-aligned nematic phase, and the perpendicular-aligned x-phase, from top to bottom. Three transient changes of molecular orientation were investigated to examine the orientational "flipping" between parallel and perpendicular or vice versa (for details refer to the text).

competing with each other, as described above. The critical shear rate $\dot{\gamma}_c$ decreases with temperature and approaches zero at 120 °C. By plotting data from our entire matrix of experiments, a mapping diagram was constructed, showing the locations of the parallel and perpendicular alignment regimes in T−$\dot{\gamma}$ space (Figure 9). Three typical WAXD patterns are also included in Figure 9, representative of the isotropic phase, parallel-oriented nematic phase, and the perpendicular-oriented x-phase.

We have examined the evolution of the molecular orientation after a jump in either temperature or shear rate from one alignment regime to the other. Three transients designed to flip the orientation were investigated: (1) fast cooling into the x-phase (130 → 110 °C, at 0.1 s^{-1}); (2) fast heating out of the x-phase (110 → 130 °C, at 0.1 s^{-1}); (3) stepping shear rate down from $\dot{\gamma} > \dot{\gamma}_c$ to $\dot{\gamma} < \dot{\gamma}_c$ in the x-phase (from 3 s^{-1} to 0.1 s^{-1}, at 110 °C), as shown in Figure 9. A temperature jump from the x-phase to the nematic phase produces a sudden change of orientation from perpendicular to parallel in less than 2 s.u., followed by a more gradual perfection of parallel alignment during prolonged shear. Both a rapid cooling into the x-phase and a step down in shear rate in the x-phase induced an almost identical response in the material as the orientation changed from parallel to perpendicular. Details of the transient change in orientation will be discussed elsewhere.[36]

3.3.3. Effect of Thermal History (x-Phase). Two *in situ* WAXD experiments were performed to examine the thermal hysteresis at a shear rate of 0.1 s^{-1} ($\dot{\gamma} < \dot{\gamma}_c$) and a temperature of 110° in the x-phase, but with different thermal histories: (a) directly heating the sample from room temperature into the x-phase followed by 30 min of thermal equilibration; (b) heating the sample to the isotropic state and then cooling it into the x-phase and holding it there for 30 min. In both cases, the initial condition shows some anisotropy ($S \neq 0$). This appears to be specific to the x-phase; a quiescent sample cooled from the isotropic state into the nematic phase shows no measurable anisotropy in WAXD. The above two experimental protocols led to quite different orientation responses in the x-phase, as shown in Figure 10. For case (a), upon flow start up, the net orientation oscillates between −0.15 and −0.05, and it stays at a low value ($S = -0.05$) up to 200 s.u. of steady shear. The diffraction pattern actually seemed to approach an isotropic ring. This does not apply to case (b), where perpendicular orientation developed gradually toward steady state. The final orientational parameter reaches a value close to −0.2, a much stronger perpendicular orientation compared to that for case (a). As shown in the previous section, powder diffraction data showed that the sample may contain some residual order in the x-phase when directly heated from room temperature into the x-phase. We believe that this residual order may explain the significant structural hysteresis phenomena on orientation development during steady shear.

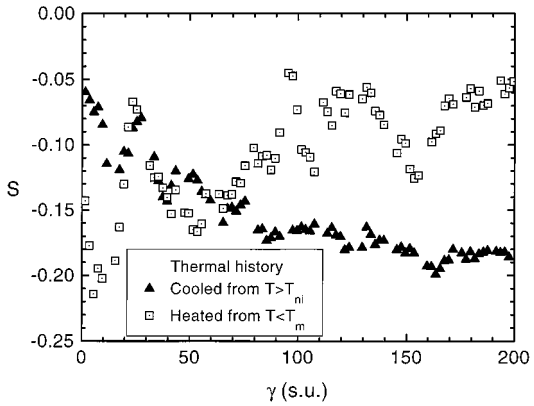

Figure 10. Effect of thermal history (residual order) on shear orientation behavior: (a) sheared after cooling from the isotropic state to the x-phase (110 °C); (b) sheared after heating from room temperature into the x-phase (110 °C). The system was subjected to steady shear at a shear rate of 0.1 s^{-1} ($\dot{\gamma} < \dot{\gamma}_c$).

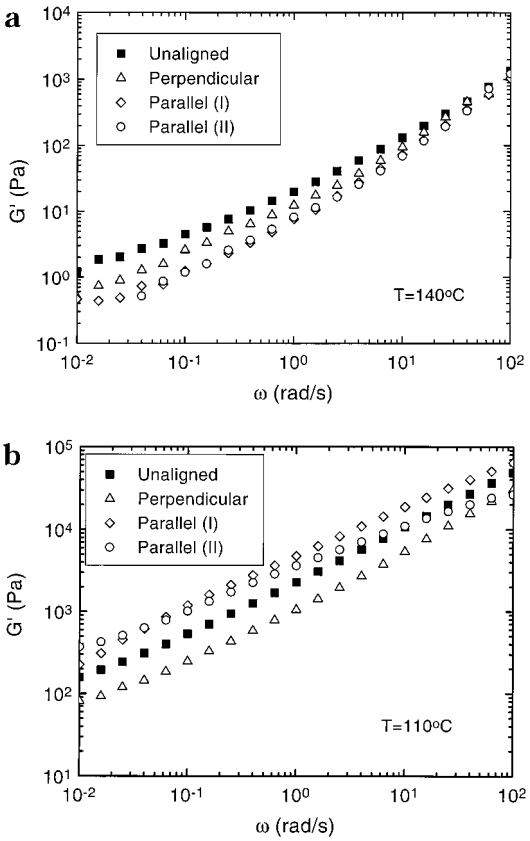

Figure 11. Effect of orientation on linear viscoelasticity behavior: (a) in the nematic phase at 140 °C; (b) in the x-phase at 110 °C. An unaligned sample was used as a reference. Two different paths of inducing parallel alignment were compared. Parallel (I): prealigned at 140 °C at the shear rate 3 s^{-1}. Parallel (II): prealigned at 110 °C at the shear rate 3 s^{-1}. Perpendicular: prealigned at 110 °C at the shear rate 0.1 s^{-1}.

3.4. Effect of Orientation on Linear Viscoelasticity. To examine the effect of alignment on linear viscoelastic properties, we prepared preferentially parallel, preferentially perpendicular and unaligned samples. Orientation was achieved by preshearing the sample at selected shear rates in the nematic or x-phase. Details of the shear and thermal histories for different orientation states are summarized in the caption of Figure 11. In the nematic phase, parallel-oriented samples were prepared in two different ways ("Parallel I", directly shearing in the nematic phase; "Parallel II", shearing at a high rate in the x-phase and then heating into the nematic phase) and perpendicular-oriented samples were prepared by shearing at a low rate in the x-phase and then heating into the nematic phase.[38] Analogously, measurements in the x-phase were performed right after steady preshearing for Parallel II and Perpendicular, and after rapidly cooling into the x-phase for Parallel I. Five minutes was allowed for thermal equilibration after a temperature jump.

The dynamic moduli in the nematic phase showed a characteristic frequency (at $\omega_c \approx 60$ rad/s), above which G' (and G'', not shown here) is insensitive to the state of alignment and below which the dynamic moduli for both parallel- and perpendicular−aligned samples are low relative to those for the unaligned state (Figure 11a). The dynamic moduli of two parallel-aligned states induced in different ways (presheared at 140 and 110 °C) are nearly the same throughout the whole frequency range, whereas the dynamic modulus of the perpendicular-aligned state falls between those of the unaligned and the parallel-aligned states. We conclude that the microstructures of two parallel-aligned samples in the nematic phase are very similar regardless of their exact thermal history.

The x-phase showed qualitatively different behavior from that of the nematic phase (Figure 11b). Most notably, the storage modulus of the parallel-aligned sample was the highest of the three states (Parallel I ≈ Parallel II > Unaligned > Perpendicular) for the x-phase, while this orientation state had the lowest modulus of the three for the nematic phase. The storage modulus of the unaligned sample lies between parallel- and perpendicular-aligned states, in contrast to having the highest G' in the nematic phase. The implications of this change in relative order of G' with orientation will be discussed in the next section.

4. Discussion

4.1. Nematic Phase. The steady shear flow behavior of nematic DHMS-7,9 shows certain similarities and differences compared to that of rigid-rod-like lyotropic LCPs. The viscosity follows a three-region flow curve, similar to that found in some commercial thermotropes[39,40] and some nematic lyotropes (such as HPC).[1] However, the value of the region II viscosity for DHMS-7,9 is much lower (about an order of magnitude) than those of commercial Vectra-type thermotropic polymers.[40] This relatively low region II viscosity reflects a difference between the materials: the present sample has lower molecular weight and greater chain flexibility (mesogen-spacer type) compared with those of commercial fully aromatic copolyesters.

While the flow curve (η versus $\dot{\gamma}$) of DHMS-7,9 shows qualitative similarities to that of lyotropic HPC, the relationship between orientation and steady shear viscosity is quite different. Lyotropic HPC shows very weak orientation in region I, an increase in orientation at the transition between regions I and II, nearly constant orientation in the plateau region II, a further increase in alignment when entering region III, and saturated orientation at high shear rate.[41] Although the lowest shear rate in our WAXD experiments did not extend far into region I, there is no indication that region I is accompanied by low orientation. Indeed, the orientation in region I is strong and there is little change with shear rate from region I to region III (Figures 6a and 8). Therefore, the qualitative understanding of the three-region flow curve in lyotropic HPC in terms of a transition from a "piled-polydomain" structure in region I, to tumbling in region II, to wagging and then flow aligning in region III cannot be invoked to explain the three-region flow curve observed in DHMS-7,9.

The relatively high and nearly constant orientation observed in steady shear may be understood in light of our recent conoscopy experiments on a monodomain sample of DHMS-7,9 (with $M_w = 11\,000$ g/mol), which indicate that DHMS-7,9 is flow-aligning.[42] Another semiflexible thermotropic system (PSHQ-6,12) also exhibits nearly constant orientation versus shear rate.[11] Indirect evidence from a simulation based on Ericksen's transversely isotropic fluid model suggests that PSHQ-6,12 is also flow-aligning,[11] in accord with its similarity to DHMS-7,9 in bulk rheology and orientation behavior. These observations suggest that mesogen-spacer type semiflexible thermotropes may generally be flow-aligning, as predicted by the nematic dumbbell model.[12]

However, for more rodlike thermotropes such as HPC, the Doi model may be more appropriate to describe their rheological behavior; in fact, recent work by Huang and co-workers has provided indirect rheological evidence that thermotropic HPC might be a tumbling nematic.[43]

The steady-state values of N_1 are positive throughout the whole shear rate range in the nematic phase. In contrast, lyotropic rodlike LCPs generally show a negative N_1 in the vicinity of the transition from region II to region III. This behavior is understood to be associated with the director "wagging" of tumbling LCPs, in which the local order parameter is perturbed by the shear flow. Given the direct evidence that DHMS-7,9 is flow-aligning,[42] a decrease of the local order parameter is not expected, and consequently, no negative values of N_1 would occur. The positive value of N_1 for semiflexible thermotropes is actually predicted by the nematic dumbbell model as a result of flow-aligning character.[12] An alternative explanation for the absence of negative N_1 has been proposed by the inclusion of viscous stress into the Doi model on the basis of the observation of a smooth upward shift of the local minimum in N_1 with the decrease of temperature in highly concentrated HPC solutions.[37] We do not believe that explanation is appropriate for DHMS-7,9 for at least three reasons: DHMS-7,9 is not rodlike due to the presence of the flexible spacers, so it does not satisfy the basic assumptions of the Doi model; secondly (and *most* importantly), DHMS-7,9 is not tumbling, while tumbling is a natural corollary of the Doi model; and thirdly, nematic DHMS-7,9 does not show the predicted local minimum in N_1.

A transition in the dependence of N_1 on shear rate occurs between regions II and III: in region II, N_1 grows almost linearly with $\dot{\gamma}$, but in region III, it increases more strongly with $\dot{\gamma}$ (Figure 6a). This behavior is reminiscent of a prediction of the nematic dumbbell model, for which N_1 initially increases linearly with shear rate but then increases quadratically once the shear rate exceeds the inverse of the chain relaxation time.[12] An upper bound on the polymer chain relaxation time in the nematic phase is inferred to be around 15 s for DHMS-7,9 on the basis of the literature value of the self-diffusion coefficient D^* ($D^* \approx 3 \times 10^{-12}$ cm^2/s for $M_w \approx 29\,000$ g/mol) and an estimate of the completely extended chain contour length l ($l \approx$ D.P. $\times$ 19.6 Å $\approx$ 650 Å for this present sample). It is reported that a semiflexible thermotrope with a very similar chemical architecture to that of DHMS-7,9 has on average one hairpin per chain.[44] This leads to a polymer relaxation time a factor of 4 smaller, around 3−4 s. The inverse of this relaxation time (τ) roughly coincides with the shear rate where N_1 starts to deviate from the linear dependence on shear rate (Figure 6a). The decrease in steady shear viscosity in region III might also be interpreted in terms of the shear rate exceeding $1/\tau$, and therefore, the change in conformation leads to the shear thinning in region III.

4.2. X-phase. The transition from the nematic to the x-phase appears to involve a very local change in fluid structure, but one that must be very subtle. This phase transition is evident calorimetrically with a very small change in enthalpy (or perhaps heat capacity only; see Figure 1). The small hysteresis associated with the nematic−x transition on heating versus cooling also indicates that this transition is very local and does not involve any significant chain rearrangement. The nature of the higher-order structure remains elusive, since no change in structure was detected by powder X-ray diffraction on cooling through T_{xn}. The small amount of higher order (weak peak at $q \approx 0.32$ Å^{-1}) observed on heating into the x-phase appears not to be crystalline, as the wide angle peak ($q \approx 1.65$ Å^{-1}) is gone even though the small angle peak persists (Figure 2c). The persistence of this small angle peak with increasing temperature suggests some kind of chain reorganization mechanism produced by crystallization, probably arising from a crystal-like repeat in the form of a mesogen-spacer unit. Such a hypothetical chain reorganization is similar to the observed nonperiodic sequence segregation in liquid crystalline random copolymers.[45] It must be emphasized again that the observed residual order on heating into the x-phase does not exist when the sample is cooled from the isotropic phase to the x-phase (Figure 2c).

The subtle structure in the x-phase has a profound effect on dynamics and shear orientation behavior. Prior diffusion measurements showed a dramatic decrease in diffusivity on moving from the nematic phase to the x-phase.[34] Our rheological results indicate a hundred-fold slowing down of the longest relaxation time (Figure 4b) and a corresponding jump in the viscosity (Figure 3) at this phase transition. Texture coarsening also reflects this dramatic increase in viscosity: while the texture in the nematic phase ($T = 160$ °C) coarsens significantly in 2 days, there is no visible coarsening in the x-phase even after 1 week. The rheo-X-ray results show a striking reversible change in the orientation in steady shear at low rates, flipping from parallel to perpendicular on cooling through T_{xn} and vice versa on heating through T_{xn}, described below.

In the x-phase, the viscosity curve shows predominantly shear thinning over the entire range of shear rate. The data display an approximately power-law relationship between η and $\dot{\gamma}$ with $\eta \sim \dot{\gamma}^{-0.56}$. This qualitative change in the shape of the flow curve with temperature across T_{xn} is reminiscent of changes reported in other thermotropic LCPs. For example, Wissbrun has studied a commercial thermotrope, which exhibited shear thinning at low temperatures, a three-region flow curve at intermediate temperatures, and more intriguing flow curves with apparent shear-thickening at even higher temperatures.[20] In the present system, the change in the shape of the flow curve is a consequence of the presence of an additional phase besides the nematic one; such complications may also occur in other thermotropes, leading to system-specific behavior due to the appearance of higher order structure (e.g., layered ordering, residual crystallinity, etc.).

The dependence of the first normal stress difference on shear rate is complicated in the x-phase: N_1 shows a local minimum with increasing shear rate. An explanation for this *shape* of $N_1(\dot{\gamma})$ has been offered for highly concentrated nematic solutions of rodlike polymers (HPC).[37] However, it should be noted that DHMS-7,9 does *not* show this behavior in its nematic phase—only in the poorly defined mesophase at lower temperature. The change in liquid crystalline order appears to be a prerequisite for the development of the local minimum in $N_1(\dot{\gamma})$ in this system. The precise structural origin of this behavior is not yet known, but it almost certainly relates to the distinctive orientational behavior observed during steady shear in the x-phase.

The most striking feature in the x-phase is the observation that two distinctive orientation states can be achieved during steady shear, depending on the applied shear rate. The transition between the parallel and perpendicular orientations observed by *in situ* WAXD agrees with neutron-scattering observations of chain anisotropy in DHMS-7,9 by Dadmun and co-workers.[46] This type of orientational flipping has been reported in two other liquid crystalline polymers: a concentrated solution of PBG and an HBA-HNA thermotropic copolyester (Vectra A900).[47,48] In both of these systems, like DHMS-7,9, this phenomenon occurred at the lower limit of the nematic temperature range. In PBG, flipping was observed just above its gelation point. In HBA-HNA, it occurred in conjunction with flow-induced crystallization; after the onset of crystallization, the orientation was almost no longer reversible from parallel to perpendicular (but not vice versa) in that system. In DHMS-7,9, residual order also has some impact on the subsequent development of orientation: samples cooled into the x-phase from T_{ni} flip reversibly, whereas samples heated into the x-phase from room temperature (containing some residual order) oriented weakly under shear; thus, the residual order seems to inhibit the process of orientation development (Figure 10).

The theoretical background for understanding orientational flipping in LCPs is based on modes of rodlike nematics.[49] However, the experimental systems which provide the closest realization of the rodlike model (e.g., PBG in *m*-cresol) do not exhibit flipping in the nematic phase. On the other hand, all the systems that do show flipping are complicated by higher-than-nematic order structure. Indeed, in the case of PBG solutions and the x-phase of DHMS-7,9, the nature of the higher order structure is not yet known. Further understanding of these more complex structures and their role on the flow-induced orientation is needed.

4.3. X-Phase: Similarities to Layered Fluids. Some of the rheological characteristics of the x-phase are reminiscent of those of lamellar block copolymers or smectic LCPs. The dynamic modulus is strongly enhanced at low frequency for the x-phase relative to the nematic phase (Figure 4c). Other systems show such a qualitative change when they self-assemble into a nanostructure which contributes slow relaxation modes.[50,51] The relative magnitudes of the storage moduli of the parallel, perpendicular, and unaligned orientation states in the x-phase are like those of layered fluids,[50] and their relative magnitudes changed to those expected for a nematic at $T > T_{xn}$. If we consider the possibility that there was some subtle smectic-like order in the x-phase, then we would expect parallel alignment to show a relatively high modulus and perpendicular alignment to give a relatively low modulus (see Figure 12b and the caption). (Note: the definition of parallel here differs from the convention in lamellar block copolymers.) For layered fluids, the unaligned state is expected to have a modulus intermediate between those for these two aligned states. This ordering of the storage moduli is observed when the respective aligned samples are characterized within the x-phase (Figure 11b). The relative ordering for the dynamic modulus expected for the nematic phase is different, since it is minimized when the director is along the flow direction (Figure 12a). For a nematic, the unaligned state is expected to have a higher modulus than either the parallel or the perpendicular aligned state. Indeed when samples of each type of orientation are characterized in the nematic phase, the relative values of the moduli accord with expectation (Figure 11a).

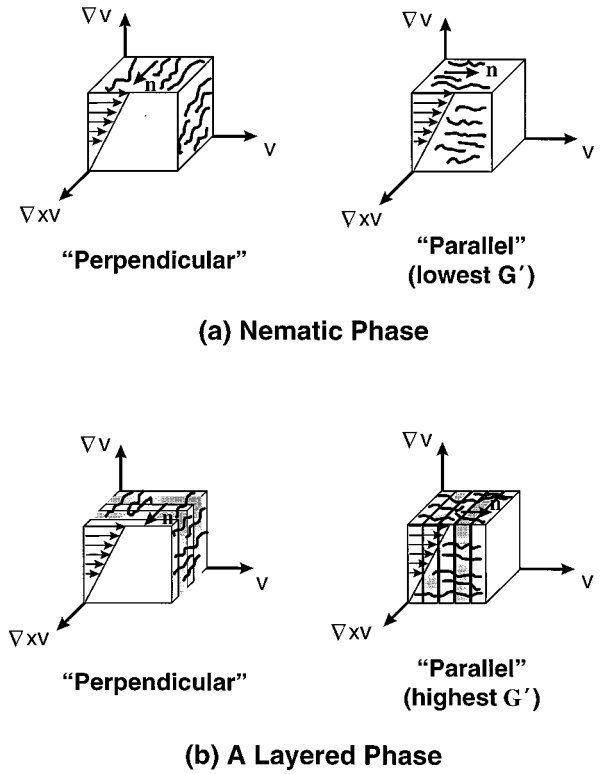

Figure 12. Schematic drawing of a tentative mechanism to explain the observed viscoelastic behavior for unaligned, parallel, and perpendicular orientation states: (a) nematic phase; (b) layered phase with lamellae on average normal to the chain axis. "Parallel" alignment corresponds to lamellae transverse to the flow; consequently, shear would distort this equilibrium layer spacing, resulting in a high modulus. "Perpendicular" alignment (director parallel to $\nabla \times \vec{v}$) corresponds to lamellae parallel to the flow plane ($\vec{v}$, $\nabla \times \vec{v}$-plane), so that this situation is not perturbed by shear even in the presence of fluctuations, and the modulus would be relatively lower.

The phase behavior and oscillatory shear alignment of a smectic layered LCP ($OQ_{OE}O10$) have been studied by Hudson and co-workers.[51,52] A similar slowing down in relaxation and enhancement in storage modulus were observed at low frequency on cooling through the nematic−smectic transition. In relation to orientation flipping, $OQ_{OE}O10$ shows strong perpendicular alignment in oscillatory shear at high frequency and/or high strain amplitude, and very weak parallel alignment at low to moderate frequency and low strain amplitude. The stability of the perpendicular alignment observed in $OQ_{OE}O10$ is said to result from minimizing the distortion of both the molecular director and the layered structures.[53]

Orientation flipping in the x-phase of DHMS-7,9 could be explained by a similar mechanism if we hypothesize that the higher order structure of the x-phase is not only subtle but also delicate. When the shear rate is below a critical value, the integrity of this order is maintained. If this higher order structure is lamellar, Hudson's explanation for the tendency toward perpendicular orientation would apply. When the shear rate is large enough to disrupt the higher order structure, the behavior reverts to that of the nematic, in which only parallel orientation was induced under shear. This

hypothesis is consistent with the observed temperature dependence of the critical shear rate in the x-phase: as temperature increases, the correlation between higher order structures presumably weakens, and as a consequence, the critical shear rate to disrupt such structures decreases. Rather than an abrupt loss of x-phase order at $\dot{\gamma}_c$, the continuous variation of η and N_1 across $\dot{\gamma}_c$ (Figure 6b) suggests a progressive erosion of the higher order structure. It appears that the x-phase structure gives rise to the high values of η and N_1 at $\dot{\gamma} < \dot{\gamma}_c$; presumably the gradual destruction of the higher order structure causes η and N_1 to drop. In particular, N_1 falls to levels consistent with the nematic phase as $\dot{\gamma}$ reaches 20 s^{-1} at 110 °C. With further increase in $\dot{\gamma}$, N_1 rises in a manner similar to the nematic phase (Figure 6), consistent with steady state values of S approaching those of the nematic phase (Figure 8, 110 °C data).

5. Conclusions

The main-chain thermotropic LCP (DHMS-7,9) showed a rich relationship between phase behavior, dynamics, and shear orientation behavior. In the nematic phase, a three-region flow curve was observed, but no negative values of N_1 were measured. WAXD studies showed that molecules tend to orient only in the flow direction under steady shear. Orientation measurements strongly suggest a flow-aligning behavior. The orientation is strong in all three regions of the flow curve; in particular, orientation is not low in region I (as would be expected in the "piled-polydomain" structure). Furthermore, there is almost no enhancement of orientation when entering region III. These results are in direct contrast with those for rigid-rod-like lyotropes (HPC).

In the poorly defined x-phase, DHMS-7,9 displays shear thinning over the whole range of shear rate and anomalous normal stress behavior, accompanied by an orientation transition from the flow direction to the vorticity direction as the shear rate decreases below a critical value. Examination of viscoelastic behavior suggests a rheological similarity between the x-phase and layered fluids. However, no direct evidence (e.g. X-ray diffraction) has been obtained for the exact mesophase ordering in the x-phase. The occurrence of perpendicular orientation is certainly related to the higher order present in the x-phase. Residual order associated with crystallinity appears not to be the cause of this orientational flipping; indeed, residual structure inhibits the perpendicular alignment process in materials heated into the x-phase.

Acknowledgment. Financial support was provided by the Air Force Office of Scientific Research (AFOSR)-LC MURI. Dow Chemical Company has generously provided us DHMS monomer. We gratefully thank Prof. C. K. Ober, Dr. S. C. Clingman (Cornell University), Prof. R. H. Grubbs, and Dr. Mike Giardello (Caltech) for help and discussion concerning scale-up of the DHMS-7,9 synthesis. Portions of this work were performed at the DuPont−Northwestern−Dow Collaborative Access Team (DND-CAT) Synchrotron Research Center located at Sector 5 of the Advanced Photon Source. DND-CAT is supported by the E.I. DuPont de Nemours & Co., the Dow Chemical Company, the U.S. National Science Foundation through Grant DMR-9304725, and the State of Illinois through Department of Commerce and the Board of Higher Education Grant IBHE HECA NWU 96. Use of the Advanced Photon Source was supported by the U.S. Department of Energy, Basic Energy Sources, Office of Energy Research, under Contract No. W-31-102-Eng-38. Part of this research was carried out at the National Synchrotron Light Source, Brookhaven National Laboratory, which is supported by U.S. DOE under Contract No. DE-AC02-98CH10886.

References and Notes

(1) Acierno, D.; Collyer, A. A. *Rheology and Processing of Liquid Crystalline Polymers*; Chapman & Hall: New York, 1996.
(2) Windle, A. H.; Donald, A. M. *Liquid Crystalline Polymers*; Cambridge University Press: Cambridge, U.K., 1992.
(3) Moldenaers, P.; Fuller, G. G.; Mewis, J. *Macromolecules* **1989**, *22*, 960.
(4) Hongladarom, K.; Ugaz, V. M.; Cinader, D. K.; Burghardt, W. R.; Quintana, J. P.; Hsiao, B. S.; Dadmun, M. D.; Hamilton, W. A.; Butler, P. D. *Macromolecules* **1996**, *29*, 5346.
(5) Walker, L. M.; Wagner, N. J.; Larson, R. G.; Mirau, P. A.; Moldenaers, P. *J. Rheol.* **1995**, *39*, 925.
(6) Doi, M. *J. Polym. Sci., Part B: Polym. Phys.* **1981**, *19*, 229.
(7) Marrucci, G.; Greco, F. *Adv. Chem. Phys.* **1993**, *LXXXVI*, 331.
(8) Burghardt, W. R.; Fuller, G. G. *Macromolecules* **1991**, *24*, 2546.
(9) Srinivasarao, M.; Berry, G. C. *J. Rheol.* **1991**, *35*, 379.
(10) Srinivasarao, M.; Garay, R. O.; Winter, H. H.; Stein, R. S. *Mol. Cryst. Liq. Cryst.* **1992**, *223*, 29.
(11) Ugaz, V. M.; Burghardt, W. R. *Macromolecules* **1998**, *31*, 8474.
(12) Maffettone, P. L.; Marrucci, G. *J. Rheol.* **1992**, *36*, 1547.
(13) Onogi, S.; Asada, T. *Rheology*; Astarita, G., Marrucci, G., Nicolais, L., Eds.; Plenum Press: New York, 1980; Vol. 1.
(14) Kiss, G.; Porter, R. S. *J. Polym. Sci.: Polym. Symp.* **1978**, *65*, 193.
(15) Moldenaers, P.; Mewis, J. *J. Rheol.* **1986**, *30*, 567.
(16) Magda, J. J.; Baek, S. G.; DeVries, K. L.; Larson, R. G. *Macromolecules* **1991**, *24*, 4460.
(17) Baek, S. G.; Magda, J. J.; Larson, R. G. *J. Rheol.* **1993**, *37*, 1201.
(18) Mewis, J.; Moldenaers, P. *Mol. Cryst. Liq. Cryst.* **1987**, *153*, 291.
(19) Moldenaers, P.; Mortier, M.; Mewis, J. *Chem. Eng. Sci.* **1994**, *49*, 699.
(20) Wissbrun, K. F. *Br. Polym. J.* **1980**, *12*, 163.
(21) Kalika, D. S.; Giles, D. W.; Denn, M. M. *J. Rheol.* **1990**, *34*, 139.
(22) Han, C. D.; Chang, S. *J. Rheol.* **1994**, *38*, 241.
(23) Greco, F.; Marrucci, G. *Liq. Cryst.* **1997**, *22*, 11.
(24) Semenov, A. N. *Sov. Phys. J. E. T. P.* **1983**, *58*, 321.
(25) Subbotin, A. *Macromolecules* **1993**, *26*, 2562.
(26) Meissner, J. *Makro. Chem. Makro. Symp.* **1992**, *56*, 25.
(27) Hsiao, B. S.; Stein, R. S.; Deutscher, K.; Winter, H. H. *J. Polym. Sci., Part B: Polym. Phys.* **1990**, *28*, 1571.
(28) Mather, P. T.; Romo-Uribe, A.; Han, C. D.; Kim, S. S. *Macromolecules* **1997**, *30*, 7977.
(29) Kim, S. S.; Han, C. D. *Macromolecules* **1993**, *26*, 6633.
(30) Driscoll, P.; Masuda, T.; Fujiwara, K. *Macromolecules* **1991**, *24*, 1567.
(31) Percec, V.; Nava, H.; Jonsson, H. *J. Polym. Sci., Part A: Polym. Chem.* **1987**, *25*, 1943.
(32) Gillmor, J. R.; Colby, R. H.; Hall, E.; Ober, C. K. *J. Rheol.* **1994**, *38*, 1623.
(33) Mitchell, G. R.; Windle, A. H. In *Developments in Crystalline Polymers*; Bassett, D. C., Ed.; Elsevier: London, 1988; Vol. 2.
(34) Hall, E.; Ober, C. K.; Kramer, E. J.; Colby, R. H.; Gillmor, J. R. *Macromolecules* **1993**, *26*, 3764.
(35) The layer spacing of 19.6 Å is approximately equal to the length of one mesogen-spacer repeating unit. The same value is used for estimation of the contour length of the polymer chains in the Discussion section.
(36) Ugaz, V. M.; Burghardt, W. R.; Zhou, W.; Kornfield, J. A. *J. Rheol.* (in preparation).
(37) Baek, S. G.; Magda, J. J.; Larson, R. G.; Hudson, S. D. *J. Rheol.* **1994**, *38*, 1473.
(38) The *in situ* rheo-X-ray observation shows that the shear-induced orientation does not relax for at least 30 min in the nematic phase and the x-phase. Thus, we assume the orientation obtained by steady preshearing in these experiments was maintained (at least qualitatively in terms of

parallel versus perpendicular) after the heating (or cooling) process and 5 min of thermal equilibration at 140 °C (or 110 °C).
(39) Giles, D. W.; Denn, M. M. *J. Rheol.* **1994**, *38*, 617.
(40) Langelaan, H. C.; Gotsis, A. D. *J. Rheol.* **1996**, *40*, 107.
(41) Burghardt, W. R. *Macromol. Chem. Phys.* **1998**, *199*, 471.
(42) Kornfield, J. A.; Zhou, W.; Burghardt, W. R. Paper 127j, AIChE National Meeting, Miami, 1998.
(43) Huang, C. M.; Magda, J. J.; Larson, R. G. *J. Rheol.* **1999**, *43*, 31.
(44) Hardouin, F.; Sigaud, G.; Achard, M. F.; Brulet, A.; Cotton, J. P.; Yoon, D. Y.; Percec, V.; Kawasumi, M. *Macromolecules* **1995**, *28*, 5427.
(45) Hanna, S.; Romo-Uribe, A.; Windle, A. H. *Nature* **1993**, *366*, 546.
(46) Dadmun, M. D.; Clingman, S. C.; Ober, C. K.; Nakatani, A. I. *J. Polym. Sci., Part B: Polym. Phys.* **1998**, *36*, 3017.
(47) Dadmun, M. D.; Han, C. C. *Macromolecules* **1994**, *27*, 7522.
(48) Romo-Uribe, A.; Windle, A. H. *Macromolecules* **1996**, *29*, 6246.
(49) Larson, R. G.; Öttinger, H. C. *Macromolecules* **1991**, *24*, 6270.
(50) Koppi, K. A.; Tirrel, M.; Bates, F. S.; Almdal, K.; Colby, R. H. *J. Phys. II* **1992**, *2*, 1941.
(51) Hudson, S. D.; Lovinger, A. J.; Larson, R. G.; Davis, D. D.; Garay, R. O.; Fujishiro, K. *Macromolecules* **1993**, *26*, 5643.
(52) Alt, D. J.; Hudson, S. D.; Garay, R. O.; Fujishiro, K. *Macromolecules* **1995**, *28*, 1575.
(53) Safinya, C. R.; Sirota, E. B.; Plano, R. J. *Phys. Rev. Lett.* **1991**, *66*, 1986.

MA990399F